Received: 27 November 2022 | Revised: 1 April 2023 | Accepted: 10 April 2023 | Published on: 1 May 2023

DOI: 10.1002/mrm.29683

RESEARCH ARTICLE

Magnetic Resonance in Medicine

Optimal flip angles for in vivo liver 3D T_1 mapping and B_{1+} mapping at 3T

Gabriela Belsley[1] | **Damian J. Tyler**[1] | **Matthew D. Robson**[1,2] | **Elizabeth M. Tunnicliffe**[1]

[1]Oxford Centre for Clinical Magnetic Resonance Research, Division of Cardiovascular Medicine, Radcliffe Department of Medicine, University of Oxford, Oxford, UK

[2]Perspectum, Oxford, UK

Correspondence
Gabriela Belsley, Oxford Centre for Clinical Magnetic Resonance Research, Division of Cardiovascular Medicine, Radcliffe Department of Medicine, University of Oxford, Oxford, UK.
Email: gabriela.belsley@siemens-healthineers.com

Funding information
Engineering and Physical Sciences Research Council (EPSRC), Medical Research Council (MRC), Grant/Award Number: EP/L016052/1; NIHR Oxford Biomedical Research Centre

Purpose: The spoiled gradient recalled echo (SPGR) sequence with variable flip angles (FAs) enables whole liver T_1 mapping at high spatial resolutions but is strongly affected by B_1^+ inhomogeneities. The aim of this work was to study how the precision of acquired T_1 maps is affected by the T_1 and B_1^+ ranges observed in the liver at 3T, as well as how noise propagates from the acquired signals into the resulting T_1 map.

Theory: The T_1 variance was estimated through the Fisher information matrix with a total noise variance including, for the first time, the B_1^+ map noise as well as contributions from the SPGR noise.

Methods: Simulations were used to find the optimal FAs for both the B_1^+ mapping and T_1 mapping. The simulations results were validated in 10 volunteers.

Results: Four optimized SPGR FAs of 2°, 2°, 15°, and 15° (TR = 4.1 ms) and B_1^+ map FAs of 65° and 130° achieved a T_1 coefficient of variation of 6.2 ± 1.7% across 10 volunteers and validated our theoretical model. Four optimal FAs outperformed five uniformly spaced FAs, saving the patient one breath-hold. For the liver B_1^+ and T_1 parameter space at 3T, a higher return in T_1 precision was obtained by investing FAs in the SPGR acquisition rather than in the B_1^+ map.

Conclusion: A novel framework was developed and validated to calculate the SPGR T_1 variance. This framework efficiently identifies optimal FA values and determines the total number of SPGR and B_1^+ measurements needed to achieve a desired T_1 precision.

KEYWORDS

B_1^+ mapping, liver, optimal flip angles, T_1 mapping, T_1 precision

1 | INTRODUCTION

T_1 mapping is a promising non-invasive biomarker for the diagnosis and stratification of liver diseases.[1–4] MOLLI T_1 values corrected for the presence of iron in the liver[5] correlate with liver fibrosis.[1] MOLLI is a repeatable and precise T_1 mapping method,[6,7] but has drawbacks. It offers limited liver coverage as it is a single slice breath-hold technique. Using single-slice T_1 mapping methods, the detection of tumors or other liver diseases affecting localized areas of the liver are likely to be missed. MOLLI acquisitions are also commonly restricted to modern scanners with access

to a cardiac license. Moreover, T_1 values measured with MOLLI are biased[8] by several factors, the largest of which are magnetization transfer[9] and T2.[8]

The variable flip angle (VFA) spoiled gradient recalled echo (SPGR) acquisition is a widely available sequence that offers the possibility of performing whole-liver T_1 mapping. Research using the VFA SPGR sequence in the brain for T_1 mapping has shown that its T_1 accuracy is strongly dependent on corrections for B_1^+ inhomogeneities.[10–14] Research on the liver using this sequence is primarily restricted to contrast studies using gadoxetic acid, some of which are starting to acquire a B_1^+ map.[15–17]

The precision of VFA SPGR 3D T_1 mapping will be largely driven by the choice of FAs and TR for the application of interest. Deoni et al.[18] showed that the two optimal angles straddle the Ernst angle and give a signal equal to 0.71 of the Ernst angle signal. Repeating the two optimal FAs was also shown to result in better T_1 precision compared to using a range of FAs symmetrically sampled around the Ernst angle. This early work, performed at 1.5T, did not yet include B_1^+ mapping for FA correction.

Given the need to acquire B_1^+ maps, the noise propagated from the B_1^+ map should also be considered when using the T_1 variance to find the optimal FAs for the VFA SPGR. For two SPGR FAs, Helms et al.[19] derived an analytical expression to calculate T_1. Lee et al.[20] used this expression to derive the variance in T_1, including the effect of variance from the B_1^+ measurement through error propagation. However, this approach is limited to two SPGR FAs. The approach of Cheng et al.[11] is valid for an arbitrary number of FAs, but uses the linear form of the SPGR steady-state equation, which has been shown by Chang et al.[21] to result in T_1 overestimates of 10%–20% for whole-brain SPGR data (1.5T, TR = 8 ms, 1 mm^3 resolution, FAs = 2°, 3°, 14°, 17°).[21]

The Fisher information matrix allows estimating the variance in T_1 for more than two FAs using the non-linear steady-state equation. Lewis et al.[22] determined the optimal SPGR FAs by minimizing a cost function given by the variance in T_1 weighted by the joint probability density of M_0 and T_1. Nataraj et al.[23] used a min-max Cramér-Rao bound to find optimal FAs and TRs for precise T_1 and T_2 estimation. The optimization was carried out over a range of T_1s, T_2s and ±10% B_1^+ inhomogeneities. Although the B_1^+ factor was included in the T_1 variance calculation, the noise in the B_1^+ map was not considered.

The work in this paper aims to define and validate a framework to calculate the B_1^+ and T_1 variance. This framework was used to find the optimal FAs for B_1^+ mapping and the VFA SPGR acquisition that result in a precise estimate of T_1 over a wide range of clinically relevant T_1s and B_1^+ inhomogeneities typically observed in the liver at 3T. A novelty in our approach for the calculation of optimal FAs is the inclusion of B_1^+ uncertainties. This allowed answering the question: Does one have a higher return in T_1 precision by investing extra breath-holds in the SPGR or the B_1^+ map? This enabled us to explore the number of breath-holds required for a target T_1 precision, given knowledge of the B_1^+ method noise and SPGR SNR. Experimental validation of the simulations was carried out in vivo, across 10 volunteers. This framework may be useful for ultra-high fields, where B_1^+ inhomogeneities extend over a larger range.

2 | THEORY

2.1 | T_1 mapping

T_1 mapping using the SPGR sequence is based on acquiring data at different FAs to reconstruct the SPGR curve and estimate the T_1 that best fits the data points. The SPGR signal assuming steady-state is:

$$S_i = M_0 \frac{1 - \exp\left(\frac{-TR}{T_1}\right)}{1 - \cos(\alpha_i)\exp\left(\frac{-TR}{T_1}\right)} \sin(\alpha_i) \quad (1)$$

where S_i is the (noiseless) signal acquired using an excitation FA of α_i, M_0 is a numerical constant including the proton density, signal decay due to $T_2^\star$ relaxation, and the B_1^- receive sensitivity; TR is the repetition time, and T_1 is the longitudinal relaxation time.

2.2 | B_1^+ mapping

B_1^+ inhomogeneities are the main source of inaccuracy in determining T_1 through Equation (1).[10–14] For B_1^+ mapping, the ratio (R) was taken between two fully relaxed signals acquired at FA $k\alpha$ ($S_{k\alpha}$) and FA α (S_α).[24] The true FA exciting the spins is estimated through Equation (2) for $k = 2$:

$$\alpha(\mathbf{r}) = \arccos\left(\left|\frac{S_{2\alpha}(\mathbf{r})}{2S_\alpha(\mathbf{r})}\right|\right) \quad (2)$$

where $\mathbf{r} = (x, y, z)$. The B_1^+ correction factor is the ratio between the true FA and the nominal FA prescribed at the scanner.

However, a non-uniform slice profile invalidates Equation (2). To correct for slice profile effects, the complex transverse signal needs to be simulated and integrated across the slice before taking the ratio of the absolute values of the signals. A look-up-table based on this procedure can be used to interpolate the acquired signal ratio and find the true FA exciting the spins.[25]

2.3 | B_1^+ map variance

The optimal pair of FAs $(\alpha, k\alpha)$ that minimize the B_1^+ factor variance is found through error propagation of the noise from FAs α and $k\alpha$ according to Equations (3) and (4)

$$\sigma_R = |R| * \sqrt{\left(\frac{\sigma_{S_{k\alpha}}}{S_{k\alpha}}\right)^2 + \left(\frac{\sigma_{S_\alpha}}{S_\alpha}\right)^2} \tag{3}$$

where $\sigma_{S_{k\alpha}}$ represents the signal noise at FA $k\alpha$. Once σ_R is determined, Equation (4) gives an estimate of the variance associated with the B_1^+ map.

$$\sigma^2_{B_1^+} = \left(\frac{\sigma_R}{\alpha_{\text{nominal}}(\partial R/\partial\alpha)_{\alpha_{\text{true}}}}\right)^2 \tag{4}$$

2.4 | T_1 variance

The optimal SPGR FAs are selected by minimizing the variance in T_1. During the fitting of the SPGR data to Equation (1), M_0 is also an unknown parameter, making the relevant parameter vector $\boldsymbol{\theta} = [M_0, T_1]$. The minimum variance in T_1 is given by the Cramér-Rao lower bound[26] (CRLB):

$$\sigma^2_{T_1} \geq \left[\mathcal{F}^{-1}(\boldsymbol{\theta})\right]_{T_1,T_1} \tag{5}$$

where $\mathcal{F}$ is the Fisher information matrix:

$$\mathcal{F}(\boldsymbol{\theta})_{k,j} = -\mathrm{E}\left[\frac{\partial^2 \ln p(\boldsymbol{y},\boldsymbol{x},\boldsymbol{\theta})}{\partial\theta_k\partial\theta_j}\right]. \tag{6}$$

The function $p(\boldsymbol{y},\boldsymbol{x},\boldsymbol{\theta})$ represents the likelihood function (Equation 7), which was modeled as a multivariate Gaussian with mean equal to the steady-state signal. The steady-state signal is a function of the independent variables of the measurement $\boldsymbol{x} = [FA, TR, B_1^+]$. The vector $\boldsymbol{y} = [y_1, y_2, .., y_n]$ represents the measurements acquired at each FA and fixed TR. The total number of measurements acquired is N. σ_i is the total noise associated with the measurement at the ith FA.

$$p(\boldsymbol{y},\boldsymbol{x},\boldsymbol{\theta}) = \left(\frac{1}{\sqrt{2\pi}}\right)^N \left(\frac{1}{\prod_{i=1}^N \sigma_i}\right) \exp\left[-\frac{1}{2}\sum_{i=1}^N \frac{1}{\sigma_i^2}(y_i - S_i(\boldsymbol{x},\boldsymbol{\theta}))^2\right]. \tag{7}$$

After taking the second derivative and the expectation in Equation (6), the Fisher information matrix simplifies to:

$$[\mathcal{F}(\boldsymbol{\theta})]_{k,j} = \sum_{i=1}^N \frac{1}{\sigma_i^2}\left(\frac{\partial S_i}{\partial\theta_k}\frac{\partial S_i}{\partial\theta_j}\right). \tag{8}$$

To find the unknown parameters M_0 and T_1, a non-linear least squares approach was applied. The residuals of the cost function were weighted by the inverse of the total noise variance in the measurement (σ_i^2). The total noise variance in Equation (9) has two contributions: the noise in the SPGR measurement (σ^{SPGR}) as well as the uncertainty propagated from the B_1^+ map measurement $(\sigma_{B_1^+})$. This latter uncertainty has been ignored in previous works.[11,22,23,27,28]

$$\sigma_i^2 = \left(\sigma^{SPGR}\right)^2 + \left(\frac{\partial S_i}{\partial\alpha_i^{true}}\alpha_i^{\text{nominal}}\sigma_{B_1^+}\right)^2 \tag{9}$$

where $\alpha^{\text{true}} = B_1^+\alpha^{\text{nominal}}$. Calculating the inverse of the Fisher information matrix using Equations (8) and (9) gives a lower bound on the T_1 variance.

2.5 | Finding the optimal FAS through a min-max approach

Min-max is commonly used in optimization problems to find a robust solution that is optimal for the worst-case over a given parameter range.[29] It finds the FA combination that results in the minimum coefficient of variation (COV) in B_1^+ or T_1 for the worst-case in the parameter range. Equation (10) illustrates the min-max approach when optimizing T_1 measurements.

$$\alpha_{\text{Optimal}} = \arg\min_{\{\alpha\}} \max_{\{B_1^+,T_1\}} CoV_{T_1}\left(\alpha, B_1^+, T_1, TR, \sigma_{B_1^+}, \sigma_{SPGR}\right). \tag{10}$$

3 | METHODS

3.1 | Simulations: Optimal FAs for T_1 mapping

Equation (10) was implemented in a custom-built script in MATLAB to find the optimal FAs to run in the VFA SPGR. The five main inputs to estimate the variance in T_1 are the T_1 range, TR, B_1^+ factor range, the associated noise in the B_1^+ map, the noise in the VFA SPGR and the (arbitrary) value of M_0. The optimal FAs were found by following the min-max approach applied to the T_1 COV across the whole T_1 and B_1^+ parameter space. We included sets of FAs with repeated measurements at the same FA, for example 2°, 3°, 15°, 15° is a valid four-FA set. The maximum FA available at the scanner console was 15° to achieve whole liver coverage within a 15 s breath-hold. The code is available here: https://github.com/gabrielaBelsley/OptimalFAs_3DT1Maps.

A population at risk for non-alcoholic fatty liver disease had MOLLI derived iron corrected values varying between 573 and 990 ms.[30] MOLLI is known to underestimate T_1[8]; thus, a conversion factor given by the ratio of 812 to 666 ms was applied resulting in a T_1 range between 700 to 1200 ms at 3T.[30,31]

Measurements indicated typical SPGR SNRs of 45 at 2° in a healthy volunteer with low body mass index (BMI), and of 25 in a higher BMI patient with liver disease. Simulations were carried out at noise levels derived from SNRs of 12.5, 25, and 50.

The B_1^+ factor range was limited between 0.59 and 1.14,[32] with 0.05 increments. An array of four different uncertainties in B_1^+ factor ranging from 4.6% to 2.3%, decreasing in increments of $1/\sqrt{N}$ with N = [2–4], were studied to explore the propagation of noise from the B_1^+ maps into the T_1 maps. The highest B_1^+ factor uncertainty of 4.6% was the worst-case across 10 volunteers, corresponding to an SPGR SNR of 19 (nominal FA = 2°, TR = 4.1 ms). Given we adopted a min-max approach, a non-homogenous distribution of the B_1^+ uncertainty was not modeled. The B_1^+ uncertainty represents the noise of the B_1^+ factor that results in the worst-case COV T_1 across the B_1^+ and T_1 parameter space.

3.2 | Simulations: Optimal FAs for the B_1^+ mapping

The optimal B_1^+ FAs are the ones that minimize the uncertainty in B_1^+. The uncertainty was calculated using an error propagation approach and validated through Monte Carlo (MC) simulations. The SNR used for both simulations was 12 at a true FA of 65°. This corresponded to the 25th quantile of the in vivo SNRs measured in the liver, across 10 healthy volunteers. For each nominal FA pair (α, $k\alpha$), the B_1^+ factor standard deviation (SD) was calculated over a range of B_1^+ inhomogeneities (0.59–1.15, steps of 0.05)[32] and k factors (1.25–4, steps of 0.25). The signals were Bloch simulated[33] for a range of FAs (1° − 360°, steps of 1°) taking into account slice profile effects of the RF pulse. Using a min-max approach, the optimal FA pair was the one that achieved the minimum B_1^+ factor uncertainty for the true B_1^+ factor that yielded the highest B_1^+ factor SD.

In the MC simulations, for each nominal FA pair and B_1^+ factor, 10 000 iterations were used to calculate the ratio and estimate the B_1^+ factor SD. The complex Bloch simulated signals were corrupted with zero mean additive complex Gaussian noise, corresponding to an SNR of 12 at a true FA of 65°. The estimated FA was found by matching the ratio of the noisy signals with an interpolated noise-free off-line ratio, calculated over the k range and true FAs up to the ambiguity angle (95° for our RF pulse). Beyond the ambiguity angle, the function corresponding to the ratio of the signals at $k\alpha$ and α is no longer injective (Supporting Information Figure S1). The B_1^+ factor deviation is the difference between the estimated B_1^+ factor and the true B_1^+ factor.

3.3 | Image acquisition and processing

To validate the simulations, imaging data were acquired from 10 healthy volunteers, 5 male and 5 female, on a 3T Siemens Prisma (Siemens Healthineers, Erlangen, Germany) scanner. Volunteers were scanned according to our institution's ethical practices.

A 2D multi-slice gradient recalled echo (GRE) EPI sequence was used for the B_1^+ mapping with fat saturation and nominal FAs of 65° and 130°. Acquisition parameters were: FOV = 450 × 366 mm^2, matrix = 64 × 52, slice thickness of 8 mm, gap of 2 mm, 15 slices, TE/TR = 11/10 000 ms without acceleration. The bandwidth (BW) was 3906 Hz/pixel to achieve a minimum echo spacing of 0.3 ms and the slices were acquired in an interleaved scheme. Each FA was acquired during a 10 s breath-hold.

A 2D multi-slice double echo spoiled GRE acquisition with magnitude and phase reconstructed data was acquired to compute a B_0 map. The B_0 map was used for distortion correction of the GRE-EPI images through *fsl fugue*[34,35] and modeling of B_0-variations through slice in the B_1^+ map calculation. The TEs were 4.78 and 7.17 ms, TR = 20 ms, FA = 15°, FOV = 450 × 380 mm^2, matrix = 64 × 54, slice thickness of 8 mm, gap of 2 mm, 15 slices, monopolar readout gradients, BW = 630 Hz/pixel, GRAPPA[36] with two times acceleration in the phase encoding direction. Data were acquired during a single breath-hold of 8.6 s.

The T_1 contrast of the liver tissue was obtained through a 3D VFA SPGR with DIXON[37] fat/water separation. Acquisition parameters were: FOV = 450 × 366 × 144 mm^3, matrix = 320 × 260 × 48, TR/TEs = 4.1/[1.23, 2.46] ms, BW = 1040 Hertz/pixel. For an SNR of 12.5, the four optimal FAs that minimized the worst-case T_1 COV were 2°, 3°, 15°, 15°. However, to calculate the SPGR SNR in vivo, a repetition at the lowest FA (where there is no contrast from vessels) was needed. Hence, it was decided to use FAs of 2°, 2°, 15°, 15° in vivo, hereafter referred to as the standard four FAs. The standard two FAs set was 2°, 15°; the three FAs set was 2°, 2°, 15° and the five FAs set was 2°, 2°, 2°, 15°, 15°. Uniformly spaced FAs of 3°, 6°, 9°, 12°, 15° (starting from the maximum FA of 15° achieved at our scanner and decreasing in increments of 3°) were also acquired. Caipirinha[38] was used with an acceleration factor of three along the slice direction with 24 separate

GRE reference lines. Spatial saturation was turned off as it perturbed the theoretical steady-state signal. Each FA is acquired independently in a breath-hold of 15 s.

The B_1^+ map was calculated with a correction for slice profile effects and off-resonance variations through slice. A non-linear least squares fit was used to find the B_1^+ correction factor corresponding to the simulated ratio that best matched the ratio between the distortion corrected GRE-EPI images acquired at nominal FAs of 130° and 65°. The simulated ratio was computed as follows: the transverse signals at each FA were Bloch simulated[33] across the slice direction, including the off-resonance at each slice position extrapolated from the B_0 map.[39] The complex transverse signal immediately after the RF pulse was propagated until time TE including free precession at the corresponding off-resonance. The complex signals at time TE were integrated across the slice dimension.

The B_1^+ map was linearly interpolated to the SPGR spatial resolution. The interpolated B_1^+ factor was multiplied by the nominal FAs to obtain the true FAs. A correction for incomplete spoiling was applied to the SPGR signal. The correction used extended phase graph simulations[40] to re-scale the signal to the theoretical steady-state value. The signal was then fit to the steady-state SPGR function through a non-linear least squares regression using MATLAB's[41] function *lsqnonlin*. Repeated FAs were not averaged prior to fitting to avoid propagating any respiratory misalignments to the average image.

3.4 | Experimental in vivo precision of the T_1 maps and B_1^+ maps

T_1 maps were analyzed by placing three circular regions of interest (ROIs) per slice, each with a radius of four pixels. The locations of these ROIs were chosen in the FA 15° SPGR image in vessel and bile free areas, avoiding the edges of the liver.

A weighted mean T_1 and SD were calculated for each subject from the T_1s extracted from each ROI selected in each slice. The weights for each ROI were given by the inverse of the standard error in the mean squared.

The acquisition of two B_1^+ maps, for each subject, enabled the calculation of the B_1^+ map precision. The three ROIs selected in each slice of the SPGR acquisition were applied to the two B_1^+ maps interpolated to the SPGR resolution. The mean B_1^+ factor was calculated for each ROI. A histogram of the liver-only portion of the B_1^+ maps was constructed with B_1^+ bins of width equal to 0.1. Using the whole liver provides enough pixels to adequately calculate the uncertainty compared to just using the pixels in each ROI. Moreover, bins were used as the B_1^+ factor uncertainty decreases with the B_1^+ factor value (Supporting Information Figure S2). The B_1^+ factor uncertainty was calculated by taking the SD of pixel-wise differences between the two binned B_1^+ maps and dividing by the square root of two. The B_1^+ factor uncertainty for each ROI was given by the B_1^+ factor SD of the bin containing the mean B_1^+ factor of the ROI.

3.5 | Prediction of in vivo T_1 precision using the CRLB

After acquiring the data, the simulations were run again to compare the CRLB derived T_1 COV against the experimental weighted T_1 COV for each subject. An estimate for the T_1 variance was calculated for each ROI. The M_0 and T_1 were set to the experimental mean value within each ROI. The mean B_1^+ factor and the associated uncertainty for each ROI were calculated as described in Section 3.4. The noise in the SPGR was calculated for each ROI from the difference between two in vivo images obtained under identical conditions at a nominal FA of 2° for the VFA SPGR, chosen to minimize the effect of vessels. A final T_1 variance for each subject was calculated from the weighted ROI T_1 variances (Supporting Information).

$$w\sigma_{T_1,\text{Simulations}} = \sqrt{\sum_{r=1}^{N_{\text{ROIs}}} w_r \left(\sigma_r^2 + \left(\mu_r - w\mu_{\text{Subject}}\right)^2\right)} \quad (11)$$

4 | RESULTS

4.1 | Simulations: Optimal FAs for T_1 mapping

Figure 1 shows how the precision varies with the total number of acquisitions for three SNR cases. Using four optimal FAs resulted in a lower T_1 COV compared to five uniformly spaced FAs of 3°, 6°, 9°, 12°, 15°. The T_1 COV for the standard FAs was comparable to that of the optimal FAs.

Figure 2 shows how the precision varies for the different T_1s and B_1^+ factors that can be measured in vivo in the liver at 3T. The worst-case T_1 imprecision corresponded to the lowest B_1^+ factor (0.59) and the lowest T_1 value (700 ms). The FA set 2°, 3°, 15°, 15° provided the minimum T_1 COV for this worst-case scenario. As the T_1 increases, the minimum T_1 COV is reached at B_1^+ factors less than 1 as the maximum sensitivity of the signal to T_1 occurs at lower FAs compared to lower T_1 values.

Table 1 shows the simulated T_1 COV obtained when using an optimal set of two, three, four, and five FAs,

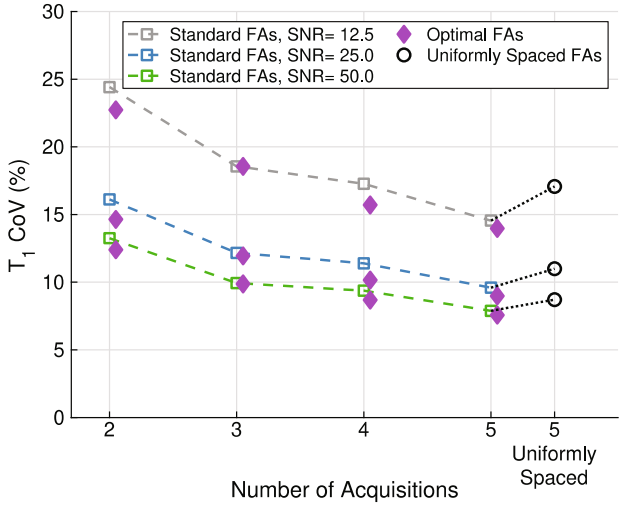

FIGURE 1 T_1 coefficient of variation (COV) as a function of the number of acquisitions (flip angles [FAs]) used to estimate T_1 for three different spoiled gradient recalled echo (SPGR) SNRs of 12.5 (gray), 25 (blue), and 50 (green), at the largest B_1^+ factor SD of 4.6%. Standard FAs (hollow squares) are compared against optimal FAs (purple diamonds) and five uniformly spaced FAs (black hollow circles). The standard two FAs set was 2°, 15°; the three FAs set was 2°, 2°, 15°; the four FAs set was 2°, 2°, 15°, 15°; and the five FAs set was 2°, 2°, 2°, 15°, 15°. The optimal FAs for each SNR are found in Table 1 and the five uniformly spaced FAs were 3°, 6°, 9°, 12°, 15°.

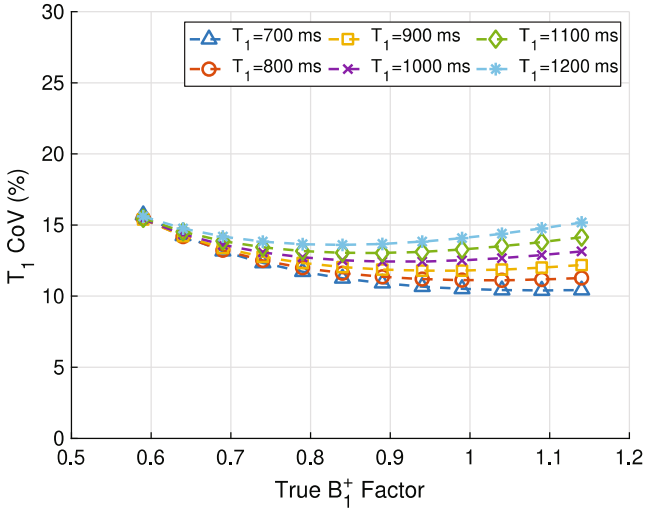

FIGURE 2 Simulated T_1 coefficient of variation (COV) as a function of T_1 and B_1^+ parameter space for four optimal flip angles (FAs) with a B_1^+ factor SD of 4.6%, and an SNR of 12.5 measured at a true FA of 2°, TR = 4.1 ms, T_1 = 800 ms, and M_0 = 5000. The smallest B_1^+ factor of 0.59 and the smallest T_1 of 700 ms were responsible for the largest T_1 COV of 15.7%. At the lowest B_1^+ factor, the T_1 COV is nearly independent of T_1, whilst for the largest B_1^+ factor the T_1 COV increases with T_1.

together with the standard FA set, using the min-max approach across a T_1 range of 700 to 1200 ms and a B_1^+ factor varying between 0.59 and 1.14 with a constant B_1^+ factor uncertainty of 4.6%, for three different SNRs.

Figure 3 shows that a larger decrease in COV T_1 is achieved by investing acquisitions in SPGR compared to investing acquisitions in the B_1^+ map, for the 3T liver parameter space explored. For example, at an SNR of 25

TABLE 1 T_1 coefficient of variation (COV) for the optimal and standard set of 2, 3, 4, and 5 acquisitions, for three different SNR values of 12.5, 25, and 50 (measured at a true flip angle [FA] = 2°, TR = 4.1 ms, T_1 = 800 ms, and M_0 = 5000) and the largest B_1^+ factor SD of 4.6%

No. of acquisitions	SNR	Optimal FA set (°)	T_1 COV (%) Optimal FA set	T_1 COV (%) Standard FA set
2	12.5	[3 13]	22.7	24.4
	25	[3 15]	14.6	16.1
	50	[4 15]	12.4	13.3
3	12.5	[2 2 15]	18.6	18.6
	25	[3 3 13]	11.9	12.2
	50	[3 3 14]	9.9	9.9
4	12.5	[2 3 15 15]	15.7	17.3
	25	[3 4 15 15]	10.2	11.4
	50	[4 5 15 15]	8.7	9.4
5	12.5	[2 2 4 15 15]	14.0	14.5
	25	[3 3 3 15 15]	9.0	9.6
	50	[3 3 4 15 15]	7.6	7.9

Note: The T_1 COV for each case corresponds to the worst-case scenario within a T_1 parameter space varying between 700 and 1200 ms and a B_1^+ factor varying between 0.59 and 1.14.

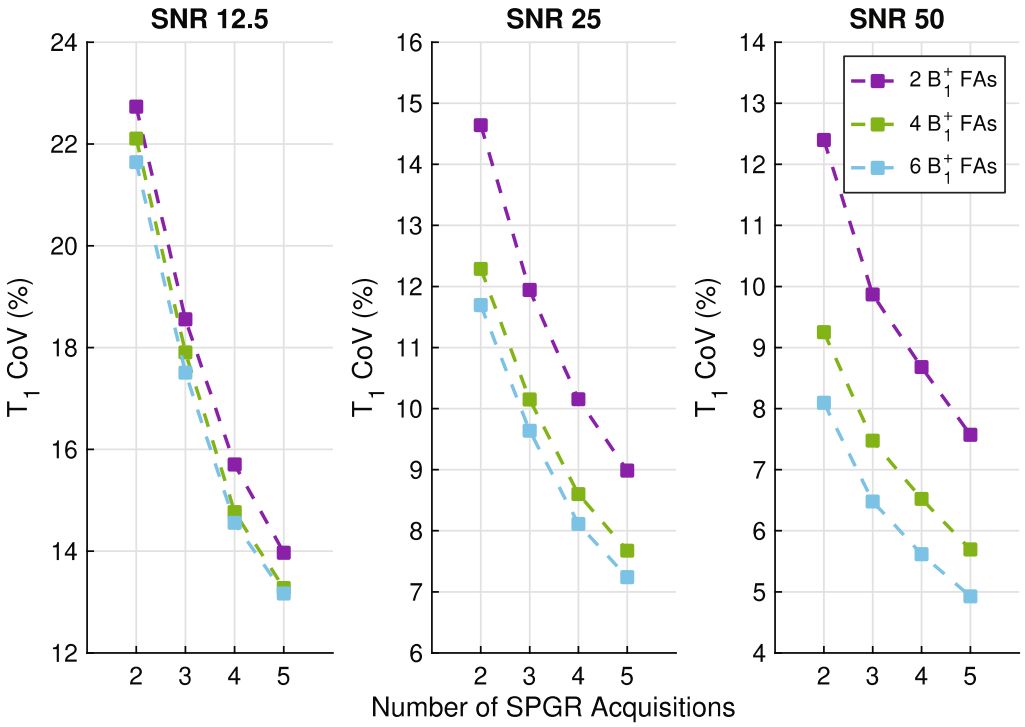

FIGURE 3 Decrease in T_1 coefficient of variation (COV) by investing acquisitions with optimal flip angles (FAs) in the spoiled gradient recalled echo (SPGR) (x axis) compared to investing two FAs (purple), four FAs (green), and six FAs (blue) in the B_1^+ map acquisition. The left, middle and right plots correspond to SPGR SNRs of 12.5, 25 and 50, respectively. There is almost always a higher return in T_1 COV when increasing the number of SPGR acquisitions compared to the number of B_1^+ map FAs. It is only best to invest in B_1^+ FAs for the case of three SPGR acquisitions and 2 B_1^+ FAs at the highest SNR. SNRs correspond to a true FA = 2°, TR = 4.1 ms, T_1 = 800 ms, and M_0 = 5000. The B_1^+ factor noise for two FAs was equal to the worst-case B_1^+ factor noise of 4.6%, for four FAs was 3.3% and for 6 FAs was 2.7%.

starting with 2 SPGR and 2 B_1^+ map FAs (14.6%), adding one more SPGR acquisition leads to a better precision (11.9%) than investing two acquisitions in the B_1^+ map (12.3%).

4.2 | Simulations: Optimal FAs for the B_1^+ mapping

An FA pair of 65°/130° minimized the uncertainty in the B_1^+ factor for the worst-case B_1^+ inhomogeneity of 0.59, confirming the optimal k factor equals 2. The uncertainty in B_1^+ factor decreased as the B_1^+ factor increased (Figure S2). 130° is the maximum FA possible at our scanner.

MC simulations confirmed the theoretical B_1^+ factor uncertainty from error propagation (Equation 4). For an in vivo SNR of 12 (nominal FA of 65°), the B_1^+ factor SD was 0.158 from the MC simulations and 0.159 from the error propagation, for the worst-case B_1^+ factor of 0.59.

Figure 4 shows the deviation of the estimated B_1^+ correction from the true B_1^+ factor for each pair of FAs, for the B_1^+ factors of 0.59, 1.0 and 1.15. The FA lower bound is influenced by the SNR, while the upper boundary is determined by the lack of phase data from this product sequence and the magnitude of the B_1^+ factor inhomogeneity.

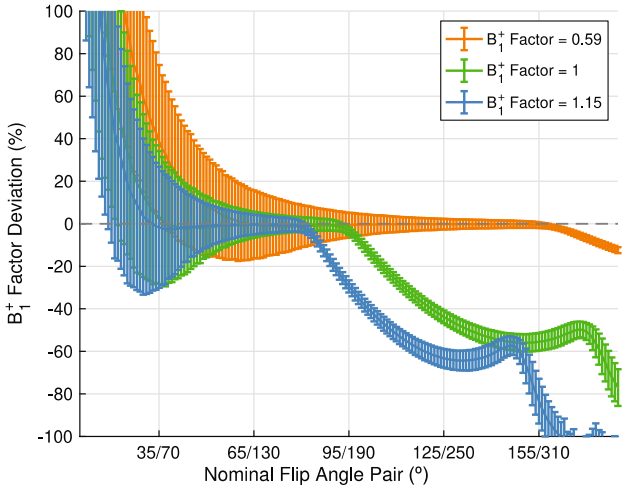

FIGURE 4 Percentage deviation in the B_1^+ factor estimate as a function of nominal flip angles (FA) pair for a B_1^+ factor of 0.59 (orange), a B_1^+ factor of 1 (green), and a B_1^+ factor of 1.15 (blue). Data from Monte Carlo simulations with 10 000 iterations. The B_1^+ factor error is above 2% for nominal FAs of 58°/116° or lower, at a B_1^+ factor of 0.59 due to low SNR. The B_1^+ factor error also deviates from 0% once the nominal FA pairs reach the ambiguity angle (function is no longer injective), which is reached first for a B_1^+ factor of 1.15 at a nominal FA pair of 83°/166°. The maximum B_1^+ factor SD one can measure is 1.46 (95°/65°).

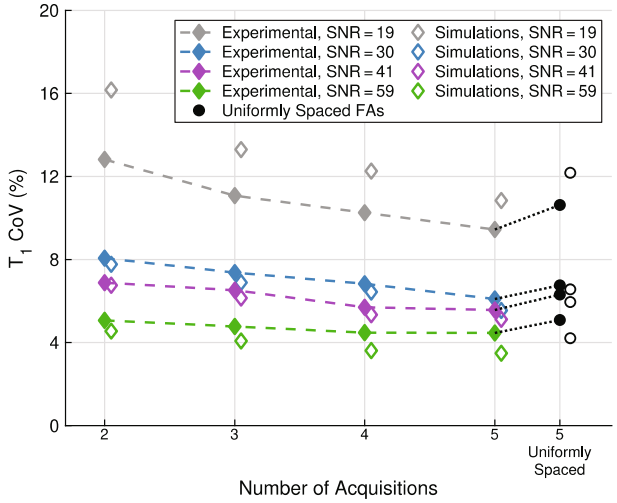

FIGURE 5 Experimental T_1 coefficient of variation (COV) as a function of the total number of acquisitions (standard flip angles [FAs]) used to estimate T_1 for four volunteers with different SPGR SNRs of 19 (gray), 30 (blue), 41 (purple) and 59 (green). The standard FAs in sets of 2, 3, 4, and 5 total FAs were [2, 15]°, [2, 2, 15]°, [2, 2, 15, 15]°, and [2, 2, 3,15,15]°, respectively. The results using five uniform FAs of [3, 6, 9, 12, 15]° are depicted in black. The filled markers represent the experimental T_1 COV, while the hollow markers, adjacent to the filled markers, correspond to the simulated T_1 COV using the experimental M_0, T_1, B_1^+ factor, spoiled gradient recalled echo (SPGR) SNR and B_1^+ factor SD obtained in vivo per regions of interest (ROIs).

4.3 | Experimental in vivo precision of the T_1 maps

Figure 5 shows how the T_1 COV varied in vivo as the number of standard FAs increased from two to five. A close agreement existed between the T_1 COV obtained in vivo and the T_1 COV simulated using the proposed algorithm, except for the lowest SNR.

The average SPGR SNR, B_1^+ map noise, mean T_1 and mean B_1^+ factor are shown in Table 2 for each volunteer. A large range of SNRs was observed from 19 to 59 and the mean B_1^+ map noise varied between 0.8% and 4.6%. The mean T_1 and B_1^+ factors varied between 775 and 1050 ms and 0.62 and 0.96, respectively. All these values, except SNRs above 50, are within the parameter space range used in the simulations.

An example of the 3D T_1 and B_1^+ maps in vivo is shown in Figure 6.

Figure 7 shows the T_1 COV experimentally decreased as the SNR increased, illustrating the large range of SNRs in the cohort of imaged volunteers. The COV in T_1, averaged across the 10 volunteers, was 6.2 ± 1.7%.

The open research question of whether a larger decrease in T_1 COV is obtained by investing extra breath-holds in the B_1^+ acquisition or the SPGR acquisition was answered in vivo by comparing the curves shown in Figure 8. It was always better to add extra breath-holds to the SPGR acquisition for the B_1^+/T_1 parameter space observed in the liver at 3T.

5 | DISCUSSION

While it is well known that the accuracy of the T_1 maps generated with the VFA SPGR is strongly dependent on the accuracy of the B_1^+ maps, what is less appreciated in the literature is how the precision of the T_1 maps are influenced by the B_1^+ map precision. In this work, we present a

TABLE 2 Characterization of spoiled gradient recalled echo (SPGR) SNR, T_1, B_1^+ factor, and B_1^+ factor noise parameter space for each volunteer

Volunteer	SPGR SNR	T_1 (ms) mean [min, max]	B_1^+ Factor mean [min, max]	B_1^+ Noise mean [min, max]
1	44	809 [619, 1070]	0.914 [0.691, 1.077]	0.028 [0.009, 0.099]
2	30	822 [621, 1054]	0.713 [0.521, 0.846]	0.012 [0.002, 0.055]
3	52	1050 [743, 1319]	0.937 [0.764, 1.020]	0.030 [0.011, 0.074]
4	51	947 [795, 1177]	0.892 [0.765, 1.101]	0.016 [0.004, 0.063]
5	59	985 [853, 1230]	0.959 [0.761, 1.086]	0.012 [0.004, 0.027]
6	34	775 [594, 1007]	0.809 [0.529, 1.003]	0.022 [0.008, 0.041]
7	41	793 [603, 978]	0.922 [0.699, 1.164]	0.016 [0.007, 0.037]
8	19	926 [626, 1341]	0.621 [0.474, 0.741]	0.046 [0.023, 0.079]
9	26	798 [607, 1091]	0.836 [0.619, 0.998]	0.026 [0.012, 0.044]
10	53	970 [802, 1157]	0.927 [0.723, 1.064]	0.008 [0.002, 0.020]

Note: The SNR is calculated from the difference of two distinct SPGR images acquired at a nominal FA of 2°. The mean, minimum, and maximum are reported for the T_1, B_1^+ factor, and B_1^+ factor noise. The mean values are weighted by one over the squared standard error of the mean T_1 within each region of interest (ROI).

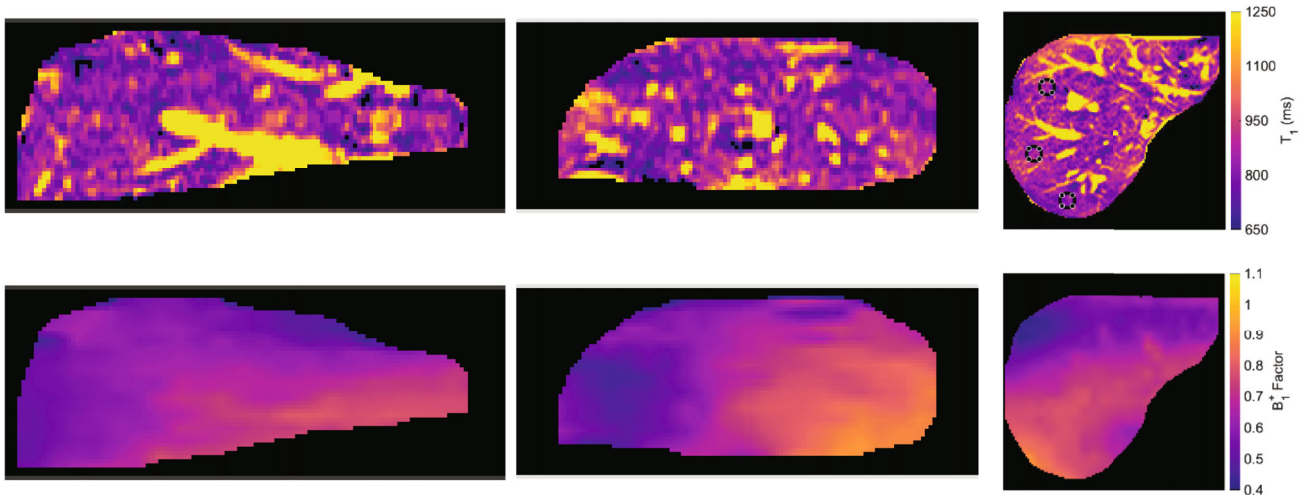

FIGURE 6 Coronal, sagittal, and axial views (with the three regions of interest [ROIs] in black) of the 3D T_1 map (first row) and B_1^+ factor map (second row) for one healthy volunteer. The vertical direction in the coronal and sagittal views corresponds to the number of slices. T_1 map scale for all views between 650 and 1250 ms. B_1^+ factor map scale for all views between 0.4 and 1.1. Supporting information shows coronal views of the 3D T_1 maps for the remaining nine volunteers.

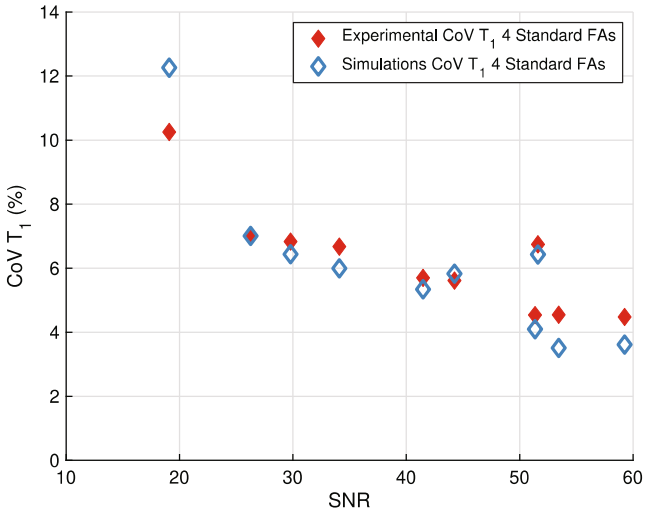

FIGURE 7 Experimental T_1 coefficient of variation (COV) as a function of SNR for the 10 volunteers. The experimental T_1 COV is shown in filled red diamonds, and the simulated T_1 COV in hollow blue diamonds for the four standard flip angles (FAs) of [2, 2, 15, 15] degrees. As the SNR increases, the T_1 COV generally decreases both experimentally and using the developed simulations algorithm. The simulated T_1 COV is in close agreement with the experimental T_1 COV.

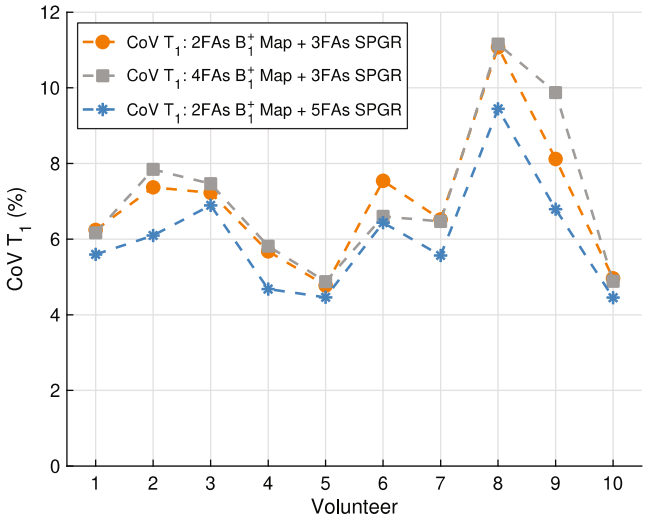

FIGURE 8 Experimental T_1 coefficient of variation (COV) using as a reference case two flip angles (FAs) in the B_1^+ map and three standard FAs in the spoiled gradient recalled echo (SPGR) acquisition (orange). Investing two more FAs in the B_1^+ map results in the gray curve, while investing two more FAs in the SPGR acquisition gives the blue curve. The in vivo data confirm the conclusions drawn from the simulation results (Figure 3) that it is best to invest FAs in the SPGR acquisition rather than the B_1^+ map. This occurs within the parameter space explored for all 10 volunteers.

quantitative model based on the Fisher information matrix to predict the variance in T_1 considering both the noise in the SPGR acquisition and the noise in the B_1^+ maps. This novel model identified the optimal set of FAs for the SPGR sequence using a min-max optimization approach on the T_1 variance across an extended range of T_1s and B_1^+ factors observed in the in vivo liver at 3T. Simulations explored the robustness of the FA choice to variations in SNR and compared optimal to standard and uniformly spaced FAs. Optimizing SPGR FA choice improves T_1 map precision and can save breath-holds. In vivo, four standard FAs resulted in better T_1 precision than five uniformly spaced FAs of [3, 6, 9, 12, 15]°. The simulation results were validated in 10 volunteers. The close agreement between

the experimental data and the simulations, within 0.5% on average, is a strong indicator that the proposed model can be used to characterize the T_1 variance and estimate optimal FAs.

The close agreement between the simulated T_1 COV, using the proposed Fisher information matrix algorithm, and the experimental data (Figure 5) for four volunteers with SNRs differing by as much as a factor of three supports the validity of our theoretical model. The largest disagreement between the experimental and simulated T_1 COV was observed for the volunteer with the lowest SNR. This volunteer, who reported falling asleep during the acquisition, had the largest B_1^+ map noise with a mean of 4.6%, almost 2.5 times higher than the average B_1^+ map noise of the other volunteers. Due to large liver misalignments (more than 1 cm between FAs was observed), the method of the differences between the two B_1^+ maps might have overestimated the B_1^+ map noise.

A rough knowledge of the in vivo SNR is helpful, but not a determining factor in finding the optimal FAs using our approach. We have shown that using the same standard FAs for all SNRs resulted in minimal increases in T_1 COV compared to the optimal FAs found for each SNR. For the liver parameter space at 3T, repeating two FAs to create a standard FA set is a robust and nearly optimal strategy. This extends Deoni's et al.[18] conclusions for situations when B_1^+ inhomogeneities and uncertainties are modeled.

The strong co-variance between T_1 and B_1^+ factor might motivate one to invest breath-holds in repeating the B_1^+ acquisition to improve T_1 precision. However, the effect of the B_1^+ map noise on the T_1 map precision depends on the B_1^+ factor noise, the SPGR noise, B_1^+ factor and T_1 range. Our simulations and experimental data showed that acquiring two extra FAs in the SPGR provided a larger reduction in T_1 COV than repeating the B_1^+ acquisition. Our comprehensive model led to the insight that acquiring extra SPGR FAs has a double effect of reducing the uncertainties in the SPGR signal and the true FAs, while repeating the B_1^+ map acquisition will only reduce the noise in the B_1^+ map. The largest in vivo B_1^+ imprecision of 4.6% was used to maximize the effect of B_1^+ noise when evaluating where to invest the breath-holds. Even with this conservative imprecision value, we found it's best to invest breath-holds in the SPGR, except possibly at very high SNRs which are unlikely in liver patients.

The main motivation for carrying out this work was to provide a framework to calculate the T_1 variance including the effects of noise that propagate from the B_1^+ maps. This allowed us to find the minimum number of acquisitions and the FA values to guarantee a target T_1 precision, even in the worst-case, across a wide range of $T_1 s$ and $B_1^+ s$ factors, given knowledge of the B_1^+ method noise and SPGR SNR. The standard set of 4 SPGR FAs (2°, 2°, 15°, 15°) and 2 B_1^+ map FAs (65°, 130°) offered a good compromise between patient comfort and the necessary T_1 precision for liver applications. Future studies will use this FA set for repeatability and clinical studies at 3T. The framework is not specific to liver applications and can be used to find the optimal compromise between the number of acquisitions and the desired precision.

5.1 | Comparison to the literature

Both Wang et al.[42] and Deoni et al.[18] offered analytical expressions for the T_1 variance and emphasized the benefits of optimizing the SPGR FAs. However, their expressions are only valid for two FAs, only consider a single T_1, omit B_1^+ inhomogeneities and rely on the linear form of the SPGR signal. Our algorithm reproduces Deoni et al.'s optimal FAs when setting B_1^+ to 1, B_1^+ noise to 0%, using a single T_1 and the maximum FA to 20°.

Cheng et al.[11] proposed the adoption of three angles for the SPGR extracted from two sets of optimal FA pairs using Deoni's approach, one optimal for the minimum T_1 and the other for the maximum T_1. This approach agrees with our findings that the largest T_1 COV is obtained for the extreme T_1s (Figure 2). However, their method to calculate the T_1 variance did not consider B_1^+ noise in the B_1^+ factor measurement. Out of the four optimal FAs, the authors advise dropping one of the lowest FAs. Our results suggest that, for the narrower range of T_1s and B_1^+s found in the liver at 3T, the optimal set of three FAs uses two low FAs, which also agrees with the results of Schabel et al.[27]

The approach by Lee et al.[20] is limited to two FAs. The authors comment in their discussion that according to their expression for T_1 variance using more than two different FAs will increase the T_1 variance. Contrary to Lee et al.[20] our results indicate, as expected, that increasing the number of distinct FAs results in a decreased T_1 COV. In the Lee et al.[20] formulation, the contribution due to the noise in the B_1^+ map is independent of the SPGR FA values. Their expression reduces to a variance in T_1 from the B_1^+ map noise given by $\sigma^2_{B_1^+} \cdot \left(-2 \cdot \mathrm{TR} \cdot \frac{T_1}{B_1^+}\right)^2$. As a result, if one were to use Lee's algorithm to find the optimal SPGR FAs, an increase in B_1^+ map noise would not change the FA values. On the other hand, our CRLB algorithm includes in the weighting factor of the cost function a B_1^+ factor noise term that varies with the SPGR FA.

Lee et al.[20] performed experimental measurements that suggest that the noise in the B_1^+ map and the noise from the individual SPGR signals, both propagated with similar weights into the T_1 map variance. For our liver parameter space at 3T, the relative contribution of the B_1^+

map noise into the T_1 variance varied significantly with the B_1^+ factor and with the SNR of the SPGR acquisition. For the lowest SNR, the T_1 variance was dominated by the SPGR noise. For the largest SNR, there was an inversion of roles with the B_1^+ factor noise dominating the T_1 variance over the SPGR noise.

Similar to those of Lewis et al.,[22] our results also suggest using two angles on either side of the Ernst angle in the steeper portion of the SPGR curve. The low FA is sensitive to M_0 and insensitive to T_1 while the high FA is sensitive to T_1 variations. The authors reported higher rat ex-vivo RMS error by 2%–3% compared to the results when using Deoni et al.'s[18] FAs, for SNRs above 5. The authors suggested that B_1^+ inhomogeneities are the cause of Deoni's FAs outperforming their optimal FAs. The authors did not consider either B_1^+ inhomogeneities or noise during FA selection. In our case, the T_1 COV of two optimal FAs selected using Deoni's criteria[18] increased the simulated T_1 COV by 4.2%, 2.9% and 1.9% for SNRs of 12.5, 25 and 50 respectively in our liver 3T parameter range (Supporting Information Table S2). Repeating Deoni's FA pair resulted in T_1 COV increases of 3.3%, 2.3% and 1.4% compared to the four optimal FAs found using our approach, for SNRs of 12.5, 25, and 50, respectively.

Our study shows that B_1^+ factors in the liver are skewed toward values below 1 (Table 2), that is, the true FA will generally be lower than the nominal FA prescribed at the scanner. This also agrees with B_1^+ factor values in the liver measured on GE scanners.[32] Nevertheless, our algorithm takes the distribution of B_1^+ factors into account when optimizing the nominal SPGR FAs.

Our approach offers several advantages. An analytical expression characterizing the variance in T_1 was developed that considers a large range of T_1 and B_1^+ factors without any approximations, simplifications, or making use of the linear form of the SPGR signal. Importantly, the analytical expression is computationally inexpensive. It overcomes the time-consuming burden of MC simulations, which can be prohibitive when including large ranges of T_1, B_1^+ factors and nominal FAs (in our case this resulted in a nine-dimensional search space with five FAs). Our method applies to any research using the SPGR signal for T_1 mapping, regardless of body part imaged or B_1^+ mapping method adopted.

Note that our approach uses the CRLB, which assumes there is no bias in the measurement of T_1. Therefore, any errors in the T_1 due to uncompensated B_1^+ inhomogeneities, incomplete spoiling,[43,44] or slice profile in 2D[25] acquisitions should be carefully considered and corrected.

6 | CONCLUSIONS

We developed a novel theoretical framework to compute the T_1 variance that incorporates for the first time both the effect of noise from the VFA SPGR signal and the B_1^+ map as well as the range of B_1^+ factors and T_1s observed in the liver at 3T. This framework efficiently identifies optimal FA values and determines the total number of SPGR measurements needed to achieve a certain T_1 COV threshold. Validation of several predictions of this robust framework was achieved in vivo by using the framework to optimize whole liver 3D T_1 mapping in vivo at 3T leading to an average T_1 COV of 6.2 ± 1.7% across 10 volunteers using a total of seven breath-holds, four standard SPGR FAs (15 s each), two B_1^+ FAs (10 s each) and one B_0 map FA (8.6 s).

DATA AVAILABILITY STATEMENT

The code for the T1 variance algorithm and used for generating the simulation results (Figures 1–3 and Table 1) is available here: https://github.com/gabrielaBelsley/OptimalFAs_3DT1Maps.

ORCID

Gabriela Belsley https://orcid.org/0000-0001-5273-2340

REFERENCES

1. Banerjee R, Pavlides M, Tunnicliffe EM, et al. Multiparametric magnetic resonance for the non-invasive diagnosis of liver disease. *J Hepatol*. 2014;60:69-77. doi:10.1016/j.jhep.2013.09.002
2. Hoad CL, Palaniyappan N, Kaye P, et al. A study of T1 relaxation time as a measure of liver fibrosis and the influence of confounding histological factors. *NMR Biomed*. 2015;28:706-714. doi:10.1002/nbm.3299
3. Pavlides M, Banerjee R, Sellwood J, et al. Multiparametric magnetic resonance imaging predicts clinical outcomes in patients with chronic liver disease. *J Hepatol*. 2016;64:308-315. doi:10.1016/j.jhep.2015.10.009
4. Palaniyappan N, Cox E, Bradley C, et al. Non-invasive assessment of portal hypertension using quantitative magnetic resonance imaging. *J Hepatol*. 2016;65:1131-1139. doi:10.1016/j.jhep.2016.07.021
5. Tunnicliffe EM, Banerjee R, Pavlides M, Neubauer S, Robson MD. A model for hepatic fibrosis: the competing effects of cell loss and iron on shortened modified look-locker inversion recovery T1 (shMOLLI-T1) in the liver. *J Magn Reson Imaging*. 2017;45:450-462. doi:10.1002/jmri.25392
6. McDonald N, Eddowes PJ, Hodson J, et al. Multiparametric magnetic resonance imaging for quantitation of liver disease: a two-Centre cross-sectional observational study. *Sci Rep*. 2018;8:1-10. doi:10.1038/s41598-018-27560-5
7. Bachtiar V, Kelly MD, Wilman HR, et al. Repeatability and reproducibility of multiparametric magnetic resonance imaging of the liver. *PLoS One*. 2019;14:1-12. doi:10.1371/journal.pone.0214921

8. Kellman P, Hansen MS. T1-mapping in the heart: accuracy and precision. *J Cardiovasc Magn Reson*. 2014;16:1-20. doi:10.1186/1532-429X-16-2
9. Robson MD, Piechnik SK, Tunnicliffe EM, Neubauer S. T1 measurements in the human myocardium: the effects of magnetization transfer on the SASHA and MOLLI sequences. *Magn Reson Med*. 2013;70:664-670. doi:10.1002/mrm.24867
10. Venkatesan R, Lin W, Haacke EM. Accurate determination of spin-density and T1 in the presence of RF- field inhomogeneities and flip-angle miscalibration. *Magn Reson Med*. 1998;40:592-602. doi:10.1002/mrm.1910400412
11. Cheng HLM, Wright GA. Rapid high-rsolution T1 mapping by variable flip angles: accurate and precise measurements in the presence of radiofrequency field inhomogeneity. *Magn Reson Med*. 2006;55:566-574. doi:10.1002/mrm.20791
12. Deoni SCL. Correction of main and transmit magnetic field (B0 and B 1) inhomogeneity effects in multicomponent-driven equilibrium single-pulse observation of T1 and T2. *Magn Reson Med*. 2011;65:1021-1035. doi:10.1002/mrm.22685
13. Stikov N, Boudreau M, Levesque IR, Tardif CL, Barral JK, Pike GB. On the accuracy of T1 mapping: searching for common ground. *Magn Reson Med*. 2015;73:514-522. doi:10.1002/mrm.25135
14. Boudreau M, Tardif CL, Stikov N, Sled JG, Lee W, Pike GB. B1 mapping for bias-correction in quantitative T1 imaging of the brain at 3T using standard pulse sequences. *J Magn Reson Imaging*. 2017;46:1673-1682. doi:10.1002/jmri.25692
15. Yoon JH, Lee JM, Kim E, Okuaki T, Han JK. Quantitative liver function analysis: volumetric T1 mapping with fast multisection B1 inhomogeneity correction in hepatocyte-specifc contrasten-hanced liver MR imaging. *Radiology*. 2017;282:408-417. doi:10.1148/radiol.2016152800
16. Haimerl M, Schlabeck M, Verloh N, et al. Volume-assisted estimation of liver function based on Gd-EOB-DTPA–enhanced MR relaxometry. *Eur Radiol*. 2016;26:1125-1133. doi:10.1007/s00330-015-3919-5
17. Kim JE, Kim HO, Bae K, Choi DS, Nickel D. T1 mapping for liver function evaluation in gadoxetic acid-enhanced MR imaging: comparison of look-locker inversion recovery and B1 inhomogeneity-corrected variable flip angle method. *Eur Radiol*. 2019;29:3584-3594. doi:10.1007/s00330-018-5947-4
18. Deoni SCL, Rutt BK, Peters TM. Rapid combined T1 and T2 mapping using gradient recalled acquisition in the steady state. *Magn Reson Med*. 2003;49:515-526. doi:10.1002/mrm.10407
19. Helms G, Dathe H, Dechent P. Quantitative FLASH MRI at 3T using a rational approximation of the Ernst equation. *Magn Reson Med*. 2008;59:667-672. doi:10.1002/mrm.21542
20. Lee Y, Callaghan MF, Nagy Z. Analysis of the precision of variable Flip angle T1 mapping with emphasis on the noise Propagated from RF transmit field maps. *Front Neurosci*. 2017;11:106. doi:10.3389/fnins.2017.00106
21. Chang LC, Cheng GK, Basser PJ, Pierpaoli C. Linear least-squares method for unbiased estimation of T1 from SPGR signals. *Magn Reson Med*. 2008;60:496-501. doi:10.1002/mrm.21669
22. Lewis CM, Hurley SA, Meyerand ME, Koay CG. Data-driven optimized flip angle selection for T1 estimation from spoiled gradient echo acquisitions. *Magn Reson Med*. 2016;76:792-802. doi:10.1002/mrm.25920
23. Nataraj G, Nielsen JF, Fessler JA. Optimizing MR scan Design for Model-Based ${T}_{1}$, ${T}_{2}$ estimation from steady-state sequences. *IEEE Trans Med Imaging*. 2017;36:467-477. doi:10.1109/TMI.2016.2614967
24. Stollberger R, Wach P. Imaging of the active B1 field. *Magn Reson Med*. 1998;35:246-251.
25. Tofts PS, Barker GJ, Parker GJM. Accurate multislice gradient echo T1 measurement in the presence of non-ideal RF pulse shape and RF field nonuniformity. *Magn Reson Med*. 2001;45:838-845. doi:10.1002/mrm.1112
26. Kay SM. *Fundamentals of Statistical Signal Processing: Estimation Theory*. Prentice-Hall PTR; 1993.
27. Schabel MC, Morrell GR. Uncertainty in T1 mapping using the variable flip angle method with two flip angles. *Phys Med Biol*. 2009;54:N1-N8. doi:10.1088/0031-9155/54/1/N01
28. Deoni SCL, Peters TM, Rutt BK. Determination of optimal angles for variable nutation proton magnetic spin-lattice, T1, and spin-spin, T2 Relaxation Times Measurement. *Magn Reson Med*. 2004;51:194-199. doi:10.1002/mrm.10661
29. Ben-Tal A, Nemirovski A. Robust solutions of uncertain linear programs. *Oper Res Lett*. 1999;25:1-13. doi:10.1016/S0167-6377(99)00016-4
30. Mojtahed A, Kelly CJ, Herlihy AH, et al. Reference range of liver corrected T1 values in a population at low risk for fatty liver disease—a UK biobank sub-study, with an appendix of interesting cases. *Abdom Radiol*. 2019;44:72-84. doi:10.1007/s00261-018-1701-2
31. Stanisz GJ, Odrobina EE, Pun J, et al. T1, T2 relaxation and magnetization transfer in tissue at 3T. *Magn Reson Med*. 2005;54:507-512. doi:10.1002/mrm.20605
32. Roberts NT, Hinshaw LA, Colgan TJ, Li T, Hernando D, Reeder SB. B0 and B1 inhomogeneities in the liver at 1.5 T and 3.0 T. *Magn Reson Med*. 2021;85:2212-2220. doi:10.1002/mrm.28549
33. Hargreaves B. Bloch Equation Simulator. http://mrsrl.stanford.edu/~brian/blochsim/. Accessed June 27, 2019
34. Smith SM, Jenkinson M, Woolrich MW, et al. Advances in functional and structural MR image analysis and implementation as FSL. *Neuroimage*. 2004;23:208-219. doi:10.1016/j.neuroimage.2004.07.051
35. Jenkinson M, Beckmann CF, Behrens TEJ, Woolrich MW, Smith SM. FSL. *Neuroimage*. 2012;62:782-790. doi:10.1016/j.neuroimage.2011.09.015
36. Griswold MA, Jakob PM, Heidemann RM, et al. Generalized autocalibrating partially parallel acquisitions (GRAPPA). *Magn Reson Med*. 2002;47:1202-1210. doi:10.1002/mrm.10171
37. Dixon T. Simple proton spectroscopic lmaging. *Radiology*. 1984;153:189-194. doi:10.1148/radiology.153.1.6089263
38. Breuer FA, Blaimer M, Heidemann RM, Mueller MF, Griswold MA, Jakob PM. Controlled aliasing in parallel imaging results in higher acceleration (CAIPIRINHA) for multi-slice imaging. *Magn Reson Med*. 2005;53:684-691. doi:10.1002/mrm.20401
39. D'Errico J. SLM-shape language modeling. MATLAB Central File Exchange. https://www.mathworks.com/matlabcentral/fileexchange/24443-slm-shape-language-modeling. Accessed April 15, 2021
40. Malik SJ, Teixeira RPAG, Hajnal JV. Extended phase graph formalism for systems with magnetization transfer and exchange. *Magn Reson Med*. 2018;80:767-779. doi:10.1002/mrm.27040
41. The MathWorks, Inc. Natick M. MATLAB Release 2019b.

42. Wang HZ, Riederer SJ, Lee JN. Optimizing the precision in T1 relaxation estimation using limited flip angles. *Magn Reson Med*. 1987;5:399-416. doi:10.1002/mrm.1910050502
43. Preibisch C, Deichmann R. Influence of RF spoiling on the stability and accuracy of T1 mapping based on spoiled FLASH with varying flip angles. *Magn Reson Med*. 2009;61:125-135. doi:10.1002/mrm.21776
44. Baudrexel S, Noth U, Schure J-R, Deichmann R. T1 mapping with the variable flip angle technique: a simple correction for insufficient spoiling of transverse magnetization. *Magn Reson Med*. 2018;79:3082-3092. doi:10.1002/mrm.26979

SUPPORTING INFORMATION

Additional supporting information may be found in the online version of the article at the publisher's website.

FIGURE S1. Ratio between the signals at FAs 2α and α, for FAs α varying between 1° and 100°. Noise in the signals results in a variation of the ratio (δR) which will correspond to a variation in the FA ($\delta\alpha$). The larger the FA, the steeper the curve. Therefore, for a fixed uncertainty in the ratio, larger FAs yield smaller uncertainties in the B_1^+ factor estimate. At a FA of 95° the function is no longer injective; the non-injectivity does not occur at 90° due to slice profile effects.

Figure S2. B_1^+ factor standard deviation as a function of B_1^+ factor values in the liver (at 3 T) for a nominal FA pair of (65°, 130°). The largest B_1^+ factor standard deviation was 0.158 and occurred for the lowest B_1^+ factor in the liver of 0.59. This curve was calculated using an SNR of 12 corresponding to the 25th quantile measured across 10 volunteers at a nominal FA of 65°.

Table S1. Comparison between T_1 CoV calculated using the CRLB and MC simulations for four optimal FAs at three different SNR levels: 12.5, 25 and 50. The SNR corresponds to a true FA = 2°, TR = 4.1 ms, T_1 = 800 ms and M_0 = 5000. For these calculations the min-max approach was followed by adopting a B_1^+ factor of 0.59 and T_1 value of 700 ms. The B_1^+ factor standard deviation was 4.6%. 50 000 iterations were used for the MC simulations.

Table S2. Comparison between T_1 CoV obtained with the optimal set of FAs proposed and the FA set using Deoni's approach,[18] for three different SNR values of 12.5, 25 and 50 (measured at a true FA = 2°, TR = 4.1 ms, T_1 = 800 ms and M_0 = 5000) and the largest B_1^+ factor standard deviation of 4.6%. The T_1 CoV for each case corresponds to the worst-case scenario within a T_1 parameter space varying between 700 and 1200 ms and a B_1^+ factor varying between 0.59 and 1.14.

Figure S3. Coronal T_1 maps for the 10 healthy volunteers showing whole liver T_1 maps. The vertical direction corresponds to the number of slices. All maps plotted with a colormap scale varying between 500 and 1500 ms.

How to cite this article: Belsley G, Tyler DJ, Robson MD, Tunnicliffe EM. Optimal flip angles for in vivo liver 3D T_1 mapping and B_{1^+} mapping at 3T. *Magn Reson Med*. 2023;90:950-962. doi: 10.1002/mrm.29683